Available online www.worldscientificnews.com

World Scientific News

An International Scientific Journal

WSN 208 (2025) 73-85 EISSN 2392-2192

Design and Mesomorphic Characterization of Cyanostilbene-6 and 3-methoxy-4-(alkyloxy)benzoic Acid-Based Liquid

Ami Yogeshkumar Patel[1]*

[1]*Department of Chemistry, Sheth P.T. Arts & Science College, Shri Govind Guru University, Godhra (389001) Gujarat INDIA

Email: amiyogeshpatel@gmail.com[1]*

ABSTRACT

A new series of liquid crystalline compounds has been synthesized by combining a Cyanostilbene-6 (CSB-6) core with alkoxy-substituted vanillic acid derivatives through ester and Schiff base linkages. The molecular design incorporates a highly conjugated and polar CSB-6 unit, known for its strong dipole moment and π–π stacking capability, along with vanillic acid moieties bearing varying alkoxy chain lengths to tune molecular flexibility and intermolecular interactions. The synthesized compounds were fully characterized using FT-IR, ^{1}H NMR, ^{13}C NMR, and elemental analysis. The mesomorphic behaviour was investigated by differential scanning calorimetry (DSC) and polarizing optical microscopy (POM). As the terminal chain length increased, a gradual shift in phase transition temperatures and the stabilization of smectic phases were observed. Additionally, density functional theory (DFT) calculations were performed to analyze the molecular geometry, dipole moment, frontier molecular orbitals, and electrostatic potential distribution provide valuable insights for the design of cyanostilbene-based mesogens.

Keywords: Cyanostilbene-6, Alkoxy vanillic acid, Mesomorphism.

(Received 22 August 2025; Accepted 18 September 2025; Date of Publication 6 October 2025)

1. INTRODUCTION

Liquid crystal materials continue to attract significant interest due to their unique combination of fluidity and long-range molecular order, making them essential in applications ranging from display technologies to organic electronics and stimuli-responsive materials. Among various classes of liquid crystalline compounds, stil-bene-based mesogens have garnered attention for their planar, π-conjugated back-bones and ease of fictionalization. In particular, cyanostilbene derivatives, which in-corporate a terminal cyano group exhibit strong dipole moments and favorable pho-tophysical properties, making them valuable scaffolds for the design of functional liquid crystalline materials [1-3]. Cyanostilbene-6 (CSB-6), a specific member of this family, features a hexyloxy-substituted phenyl ring on one end and a cyano-functionalized vinylene bridge on the other. This molecular architecture facilitates strong dipole–dipole interactions and π–π stacking, both of which are crucial for the formation and stabilization of mesophases. Furthermore, the extended conjugation enhances optical activity, fluorescence, and molecular polarizability, making CSB-6 an excellent core for constructing multifunctional liquid crystals [4-10].On the other hand, vanillic acid derivatives, characterized by their 3-methoxy-4-hydroxybenzene moiety, offer enhanced versatility in molecular design. The methoxy group introduces lateral electronic effects and steric bulk, while the hydroxyl group provides a convenient handle for further derivatization, such as esterification or Schiff base formation. When alkoxy chains of varying lengths are introduced at the phenolic position, they effectively tune the flexibility, anisotropy, and phase transition behavior of the resulting mesogens. Moreover, the introduction of alkoxy chains (CnH2n+1O–) on the vanillic acid unit can modulate van der Waals interactions and influence thermal stability and phase range [11-14]. In this context, the present work focuses on the design, synthesis, and characterization of a novel series of Schiff base ester-linked liquid crystalline compounds derived from cyanostilbene-6 (CSB-6) and alkoxy-substituted vanillic acids, as mentioned in Scheme 1.

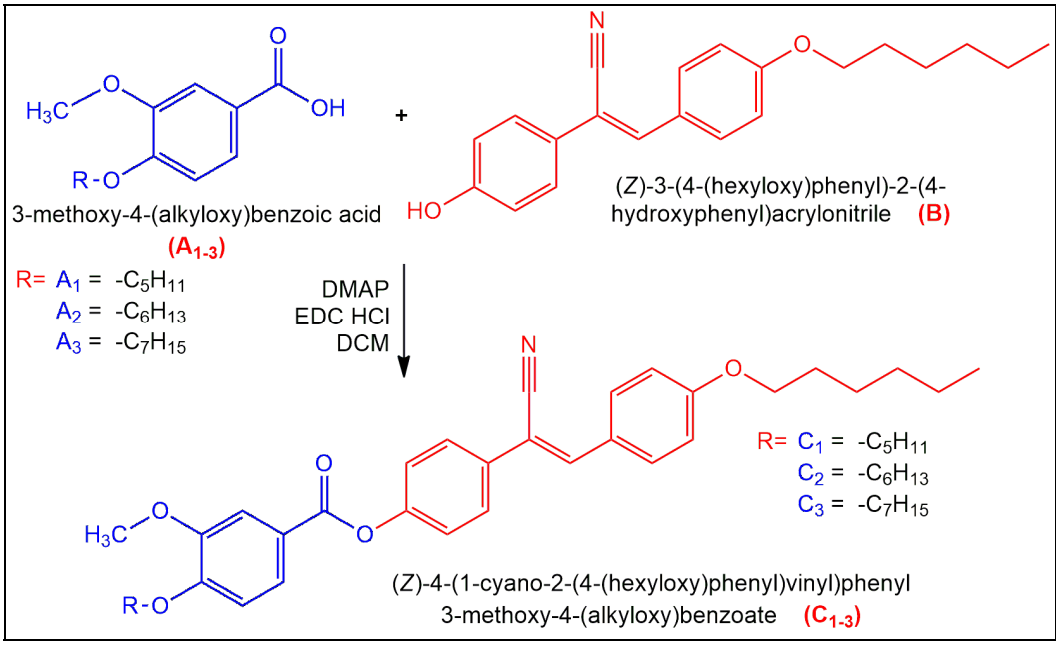

Scheme 1. Synthetic route of Compounds.

The rationale behind this molecular design is to combine the rigidity and dipolar na-ture of the CSB-6 core with the flexible, tunable side chains of vanillic acid deriva-tives, thereby achieving desirable mesophase behavior and enhanced thermal properties. To evaluate the structure–property relationships, a systematic variation in the alkoxy chain length (C5–C7) was introduced. The mesomorphic behavior of the synthesized compounds was thoroughly examined using polarizing optical microscopy (POM) and differential scanning calorimetry (DSC). The impact of molecular length, lateral substitution, and electronic effects on the type, temperature range, and stability of mesophases was analyzed. Furthermore, spectroscopic analyses were employed to confirm the structural integrity of the compounds. To gain additional insight into molecular polarity and reactivity, computational methods including Density Functional Theory (DFT) calculations, HOMO–LUMO energy gap analysis, and Molecular Electrostatic Potential (MEP) mapping were also performed. Scheme 1 represents the synthetic route of the compounds.

2. EXPERIMENTAL

All chemicals were of analytical grade. Solvents were dried and distilled following standard procedures prior to use. Proton nuclear magnetic resonance (^{1}H NMR) and Carbon nuclear magnetic resonance (^{13}C NMR) spectra were obtained using a Bruker Avance III™ HD 500 MHz spectrometer (Bruker Corporation, USA), with $CDCl_3$ as the solvent and tetramethylsilane (TMS) as the internal standard. Fourier-transform infrared (FT-IR) spectra were recorded using the ATR method over the range of 400–4000 cm^{-1} on a Nicolet-760 FT-IR spectrophotometer (Canada). Differential Scanning Calorimetry (DSC) measurements were carried out using a DSC 4000 Thermal Analyzer (PerkinElmer Inc., CA, USA). Polarizing optical microscopy (POM) was employed to study surface textures in the heating stage under finite temperature conditions using a Nikon Eclipse LV-100POL microscope equipped with a CFI60 infinity optical system (Nikon Instruments Inc., NY, USA).

Synthesis of (Z)-3-(4-(hexyloxy)phenyl)-2-(4-hydroxyphenyl)acrylonitrile (B)

In a dry 100 mL round-bottom flask fitted with a magnetic stirrer and reflux condenser, dissolve 4-hydroxyphenylacetonitrile (5.00 mmol) and 4-(hexyloxy)benzaldehyde (5.00 mmol) in 20 mL absolute ethanol. Add piperidine (0.25 mmol) and acetic acid (0.25 mmol). Heat the reaction mixture to reflux (at around 70 °C) with stirring for 3–6 h. Monitor the reaction by TLC (hexane:EtOAc 8:2) [15]. The reaction commonly forms the (Z)-isomer predominantly under these conditions. After completion by TLC, cool the mixture to room temperature. Remove solvent under reduced pressure (rotary evaporator).Add 25 mL of water to the residue and extract with ethyl acetate (3 × 30 mL). Combine organic layers, wash with brine (20 mL), dry over anhydrous Na_2SO_4, filter and concentrate under reduced pressure. Purify the crude product by column chromatography on silica gel (hexane → hexane/EtOAc 95:5 to 9:1) and recrystallization from ethanol/hexane to afford the desired (Z)-acrylonitrile as a solid.

(Z)-3-(4-(hexyloxy)phenyl)-2-(4-hydroxyphenyl)acrylonitrile (B): M.F.: $C_{21}H_{23}NO_2$; M.Wt.: 321.41 g/mol; Yield: 60%. Mp: 118–120°C; ^{1}H NMR (400 MHz, $CDCl_3$) δ: 8.03 (d, 1H, CH=), 7.64 (d, 2H, Ar–H, of 4-hydroxyphenyl), 7.15 (d, 2H, Ar–H, H-3′/5′ of 4-hydroxyphenyl), 7.08 (d, J = 8.8 Hz, 2H, Ar–H), 6.88 (d, J = 8.8 Hz, 2H, Ar–H), 10.21 (s, 1H, OH), 4.04 (t, J = 6.6 Hz, 2H, OCH_2), 1.85 (q, J ≈ 6.8 Hz, 2H, CH_2), 1.46–1.22 (m, 8H, CH_2 chain), 0.88 (t, J = 6.8 Hz, 3H, CH_3); ^{13}CMR (100 MHz, $CDCl_3$) δ: 162.0 (C–OH), 159.6 (C–O), 150–140 (Ar/C=C), 133.4, 131.2, 128.9, 127.4, 123.8, 119.6, 117.2 (C≡N), 114.3, 68.5 (OCH_2), 31.9, 29.6, 29.4, 26.2, 22.8, 14.0 (CH_3); FTIR (KBr cm^{-1}): 3425 (br, O–H), 2923, 2854 (C–H, aliphatic), 2225 (C≡N), 1605, 1510 (aromatic C=C), 1240 (C–O–C), 827 (aromatic C–H out-of-plane); CHN analysis, calculated % (found %): C, 78.47 (78.35); H, 7.21 (7.14); N, 4.36 (4.22); O, 9.96(9.82).

Synthesis of 3-methoxy-4-(alkyloxy)benzoic acid (A_{1-3})

3-methoxy-4-(alkyloxy) benzoicacid derivatives **A_{1-3}** were synthesized using reported method [13-14]. Where, A_1= 3-methoxy-4-(pentyloxy)benzoic acid; A_2= 4-(hexyloxy)-3-methoxy benzoic acid; A_3= 4-(heptyloxy)-3-methoxybenzoic acid.

Synthesis of (Z)-4-(1-cyano-2-(4-(hexyloxy)phenyl)vinyl)phenyl 3-methoxy-4-(alkyloxy) benzoate (C_{1-3})

To a stirred solution of alkoxy-vanillic acid (0.55 g, 2.0 mmol) and (Z)-3-(4-(hexyloxy)phenyl)-2-(4-hydroxyphenyl)acrylonitrile (0.50 g, 1.82 mmol) in dry DCM (20 mL) at 0 °C under N_2 was added EDCI·HCl (0.35 g, 1.82 mmol) and DMAP (22 mg, 0.18 mmol). The reaction was allowed to warm to room temperature and stirred for 6 h. Reaction progress was monitored by TLC (Hexane : Ethyl acetate = 7:3). After completion, the mixture was diluted with DCM (30 mL), washed with 1 M HCl (2 × 15 mL), saturated $NaHCO_3$ (15 mL) and brine (15 mL). The organic layer was dried (Na_2SO_4), filtered, and concentrated under reduced pressure. The crude product was purified by column chromatography (silica; hexane/EtOAc 9:1 → 8:2) to give the esterified product as a pale yellow solid (yield 70%).

C1: (Z)-4-(1-cyano-2-(4-(hexyloxy)phenyl)vinyl)phenyl 3-methoxy-4-(pentyloxy) benzoate

M.F.: $C_{34}H_{39}NO_5$; M. Wt. 541.68 g/mol; Yield: 60 %; ^{1}H NMR (400 MHz, $CDCl_3$) δ: 7.92–6.78 (m, Ar–H, 12H), 7.65 (s, –CH=), 4.03 (t, J = 6.4 Hz, –OCH_2–, 2H), 3.96 (t, J = 6.4 Hz, –OCH_2–, 2H), 1.83–1.25 (m, –(CH_2)n–, 22H), 0.89 (t, J = 6.8 Hz, –CH_3, 6H);^{13}C NMR (100 MHz, $CDCl_3$) δ: 163.5 (C=O), 161.8, 157.2, 151.6, 147.8, 134.6, 132.2, 130.7, 128.9, 124.5, 120.7, 116.2 (CN), 115.5, 113.8 (Ar–C), 67.1, 66.8 (–OCH_2–), 32.0, 30.7, 29.4, 26.1, 22.7 (–CH_2–), 14.1 (–CH_3); FTIR (KBr, cm^{-1}): 2925, 2854 (aliphatic C–H), 2222 (–C≡N), 1719 (C=O), 1605 (C=C aromatic), 1514, 1462 (Ar–C=C), 1256 (C–O–C), 835 (p-substituted aromatic).CHN analysis, calculated % (found %): C, 75.39 (75.03); H, 7.26 (7.19); N, 2.59 (2.51); O, 14.77 (14.62).

C2: (Z)-4-(1-cyano-2-(4-(hexyloxy)phenyl)vinyl)phenyl 4-(hexyloxy)-3-methoxy benzoate

M.F.: $C_{35}H_{41}NO_5$; M. Wt. 555.70 g/mol; Yield: 62%; ^{1}H NMR (400 MHz, $CDCl_3$) δ: 7.92–6.78 (m, Ar–H, 12H), 7.65 (s, –CH=), 4.04 (t, J = 6.4 Hz, –OCH_2–, 2H), 3.96 (t, J = 6.4 Hz, –OCH_2–, 2H), 1.85–1.25 (m, –(CH_2)n–, 26H), 0.88 (t, J = 6.8 Hz, –CH_3, 6H); ^{13}C NMR (100 MHz, $CDCl_3$) δ: 163.4 (C=O), 161.9, 157.3, 151.5, 147.9, 134.7, 132.3, 130.8, 128.8, 124.6, 120.6, 116.1 (CN), 115.6, 113.9 (Ar–C), 67.2, 66.9 (–OCH_2–), 32.1, 30.8, 29.5, 26.2, 22.7 (–CH_2–), 14.1 (–CH_3); FTIR (KBr, cm^{-1}): 2926, 2855 (aliphatic C–H), 2223 (–C≡N), 1720 (C=O), 1604 (C=C aromatic), 1515, 1461 (Ar–C=C), 1257 (C–O–C), 836 (p-substituted aromatic); CHN analysis, calculated % (found %): C, 75.65 (75.53); H, 7.44 (7.39); N, 2.52 (2.48); O, 14.40 (14.31).

C3:(Z)-4-(1-cyano-2-(4-(hexyloxy)phenyl)vinyl)phenyl 4-(heptyloxy)-3-methoxy benzoate: M.F.: C36H43NO5; M. Wt. 569.73 g/mol; ^{1}H NMR (400 MHz, $CDCl_3$) δ: 7.93–6.80 (m, Ar–H, 12H), 7.64 (s, –CH=), 4.05 (t, J = 6.4 Hz, –OCH_2–, 2H), 3.97 (t, J = 6.4 Hz, –OCH_2–, 2H), 1.86–1.25 (m, –(CH_2)n–, 28H), 0.89 (t, J = 6.8 Hz, –CH_3, 6H); ^{13}C NMR (100 MHz, $CDCl_3$) δ: 163.5 (C=O), 161.8, 157.4, 151.6, 147.8, 134.9, 132.5, 130.7, 128.7, 124.7, 120.5, 116.2 (CN), 115.7, 114.0 (Ar–C), 67.3, 67.0 (–OCH_2–), 32.2, 30.9, 29.6, 26.3, 22.8 (–CH_2–), 14.1 (–CH_3); FTIR (KBr, cm^{-1}): 2924, 2853 (aliphatic C–H), 2223 (–C≡N), 1721 (C=O), 1606 (C=C aromatic), 1516, 1460 (Ar–C=C), 1258 (C–O–C), 838 (p-substituted aromatic); CHN analysis, calculated% (found %): C, 75.89 (75.77); H, 7.61 (7.55); N, 2.46 (2.41); O, 14.04 (14.0).

Characterization of mesomorphic and computational properties

POM was employed to observe textures and identify mesophases of the liquid crystalline samples, while DSC provided melting points, phase transition temperatures, enthalpy changes (ΔH), and thermal behavior. Additionally, DFT analysis was used to investigate molecular geometry, electronic properties, and HOMO–LUMO energy levels of the Schiff base derivatives.

3. RESULTS AND DISCUSSION

Structural elucidation of B and C_{1-3}

The spectral data of the three homologues (C5, C6, and C7) confirm the successful incorporation of the alkoxy chain length variation. In the ^{1}H NMR spectra, all three compounds displayed characteristic aromatic proton multiplets in the range δ 7.90–6.80 and the azomethine (–CH=N–) singlet at δ 7.64, confirming the Schiff base linkage. The terminal methoxy protons appeared consistently as triplets around δ 4.05–3.97 (–OCH_2–), while the aliphatic methylene resonances broadened progressively downfield with chain elongation: C5 showed δ 1.85–1.24, C6 δ 1.85–1.26, and C7 δ 1.86–1.25. The terminal methyl triplets at δ 0.89 (–CH_3) were observed in all compounds. Similarly, ^{13}C NMR spectra displayed consistent signals for the ester carbonyl carbon (δ 163.5), azomethine and aromatic carbons (δ 161.8–114.0), and nitrile carbon (δ ~116.2), with systematic increases in the number of aliphatic carbons from C5 to C7, as evidenced by additional methylene carbon signals at δ 32.2–22.8 and terminal methyl at δ 14.1. FTIR spectra of all three compounds exhibited strong absorptions at 2924–2853 cm^{-1} (aliphatic C–H), 2223 cm^{-1} (–C≡N), and 1721 cm^{-1} (C=O stretching), along with characteristic aromatic absorptions at 1606, 1516, and 1460 cm^{-1} and ether bands near 1258 cm^{-1} [16-17].

A clear trend is observed with increasing alkoxy chain length: while the aromatic and azomethine regions remain unchanged, the intensity and multiplicity of methylene absorptions in both $^{1}H/^{13}C$ NMR and the aliphatic C–H stretching bands in FTIR systematically increase, reflecting the longer flexible alkyl chains. The comparative spectral analysis of (Z)-3-(4-(hexyloxy)phenyl)-2-(4-hydroxyphenyl)acrylo-nitrile and its final product, obtained via condensation with alkoxy vanillic acid, reveals distinct changes in NMR, CMR, and FTIR data, confirming successful product formation. In the ^{1}H NMR spectrum**,** the starting material exhibits characteristic olefinic proton signals (–CH=CH–) in the downfield region (~δ 7.5–6.8 ppm) and a singlet corresponding to the phenolic –OH (~δ 9.5–10.0 ppm) [18]. Upon reaction, the olefinic proton signals undergo slight downfield shifts due to extended conjugation, while additional aromatic and methoxy signals from the alkoxy vanillic acid moiety appear (~δ 3.8–4.0 ppm for OCH_3 and δ 0.8–1.8 ppm for $–(CH_2)_n–$ of the alkoxy chain) [13]. The phenolic OH broad signal in the starting material may shift or broaden further due to intramolecular hydrogen bonding in the final product. ^{13}C NMR (CMR) spectra also display notable changes: the starting material shows a nitrile carbon resonance around δ 115–118 ppm and olefinic carbons between δ 120–145 ppm, while the final product reveals additional aromatic carbons from the vanillic acid unit, an upfield signal for methoxy carbon (~δ 55–57 ppm), and alkoxy chain carbons in the δ 14–35 ppm range. FTIR spectra further confirm the transformation: the nitrile stretching band (~2220 cm^{-1}) in the starting material is retained but may shift slightly due to altered electronic environments; the strong phenolic O–H stretch (~3400 cm^{-1}) is still present but broadened in the final product; and new C–O–C stretching bands (~1240–1270 cm^{-1}) and aromatic ether absorptions emerge due to the alkoxy vanillic acid incorporation [14, 19]. Together, these spectral changes across ^{1}H NMR, ^{13}C NMR, and FTIR unambiguously confirm the structural modification of the starting acrylonitrile derivative into the desired alkoxy-vanillic acid conjugated product.

Polarized Optical Microscopy (POM) Observation

Under polarized optical microscopy (POM), distinct differences were observed in the mesophase textures of C1 (C5), C2 (C6), and C3 (C7) as shown in Figure 1.

Figure 1. POM of Compound C1 to C3.

Compound C1 (C5) exhibited bright, high-contrast birefringence with fine granular or mosaic domains, indicative of strong optical anisotropy and long-range molecular order. The sharp domain boundaries suggest a highly ordered smectic (A/C) phase or a well-aligned nematic state just below the clearing transition, stabilized by strong π–π interactions of the cyanostilbene core with minimal dilution from the short alkoxy chain. In contrast, C2 (C6) displayed smoother, more homogeneous textures with moderate birefringence, characteristic of nematic order or a weak smectic A phase with merged domains. The additional –CH_2– group increases conformational flexibility, slightly reducing birefringence but yielding a more uniform texture. C3 (C7) showed the weakest birefringence, presenting a dull, coarse texture with diminished contrast, consistent with a weakly ordered nematic state approaching the isotropic transition. The systematic trend in birefringence intensity and apparent order (C5 > C6 > C7) reflects the influence of alkoxy chain elongation, where increased flexibility and free volume disrupt tight π–π stacking, reduce the correlation length, and dampen optical anisotropy. Such behavior aligns with the general observation that rod-like mesogens often display optimum mesomorphic stability at intermediate chain lengths, beyond which longer chains act as internal diluents, weakening mesophase order and lowering birefringence at a given temperature [20-23]. The thermal and optical analyses of the synthesized compounds exhibit a strong correlation between the DSC thermogram of C3 and POM observations, confirming their mesomorphic behavior. In the DSC traces, sharp endothermic peaks at lower temperatures correspond to the melting of crystalline domains, which is further supported by the birefringent and mosaic-like textures observed under POM, as seen in sample C1. Subsequent minor transitions in the DSC profile attributed to the crystalline-to-smectic transformation are consistent with the fan-shaped and focal-conic textures displayed in POM images, particularly in C2, confirming smectic ordering. At higher temperatures, the broad DSC transition plateau before clearing aligns with the appearance of schlieren and thread-like textures under POM (C3), characteristic of nematic phases. Finally, the broad endothermic peak corresponding to the clearing point (N→Iso) in DSC matches the disappearance of birefringence under POM, indicating the isotropic liquid phase. Thus, the agreement between DSC thermal transitions (Cr→Sm→N→Iso) and the corresponding optical textures observed in POM provides conclusive evidence of the liquid crystalline nature of these compounds.

Thermal Analysis by Differential Scanning Calorimetry (DSC)

The DSC thermogram of C7 (Figure 2) demonstrates a sequence of thermal events typical for liquid crystalline materials, revealing the nature of its mesophases and molecular packing. Initially, at low temperature (0–3 min), the compound exists in a crystalline state, where the molecules are highly ordered. Around 3–6 min, two distinct sharp endothermic peaks are observed, which correspond to melting transitions. These peaks suggest the presence of crystalline polymorphism or multiple crystalline domains (Cr1→Cr2→Sm/N), where the compound undergoes stepwise melting before reaching a mesophase. The sharpness of these peaks reflects the significant enthalpy change associated with breaking strong intermolecular interactions within the crystalline lattice. After melting, a nearly stable baseline is observed between ~6–25 min, indicating the stability of an intermediate mesophase.

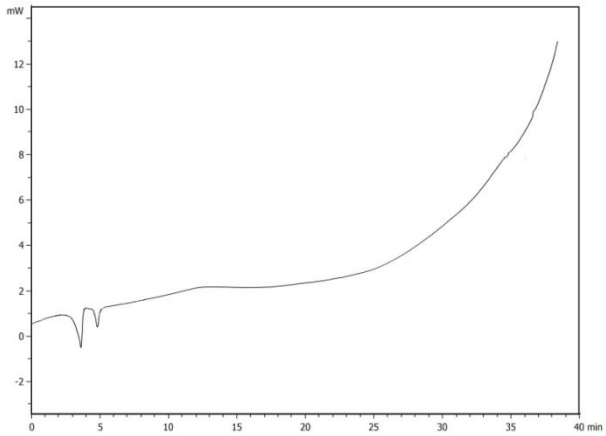

Figure 2. DSC of Compound C3.

This plateau region represents the persistence of liquid crystalline ordering, most likely smectic or nematic, depending on molecular arrangement and alkyl chain length. The mesophase stability in this interval confirms that the compound does not immediately transform into the isotropic state but instead retains partial ordering of its molecules. As the temperature rises further (25–35 min), a broad endothermic transition is recorded, attributed to the mesophase-to-isotropic phase change (Sm/N → Iso). Unlike the sharp melting peaks, this broad and diffuse transition suggests a gradual loss of long-range orientational and positional order. The reduced enthalpy associated with this process is characteristic of mesophase clearing, where the molecular interactions weaken progressively rather than abruptly. The increasing baseline slope in this region also reflects enhanced molecular motion and thermal expansion as the system approaches isotropy. Finally, beyond ~35 min, the curve rises steeply, representing the isotropic liquid phase with no ordered arrangement of molecules. The overall DSC profile of C7 thus indicates: Crystalline phase transitions: multiple sharp endothermic peaks (Cr → Cr/Sm/N).Stable mesophase region: broad plateau (~6–25 min).Diffuse clearing point: broad endothermic peak (25–35 min, Sm/N → Iso).This behavior is consistent with long-chain Schiff base derivatives, where extended alkyl chains enhance van der Waals interactions, stabilize mesophases, and broaden the clearing transition. The DSC analysis therefore confirms the liquid crystalline character of C7, with distinct crystalline melting and mesophase-to-isotropic transition.

Frontier molecular orbitals (FMOs') and Reactivity Parameters:

The frontier molecular orbital (FMO) analysis and density functional theory (DFT) calculations were carried out to evaluate the electronic properties of compounds C1–C3. The spatial distributions of the HOMO and LUMO orbitals are presented in Figure 3, while the calculated electronic parameters are summarized in Table 1.

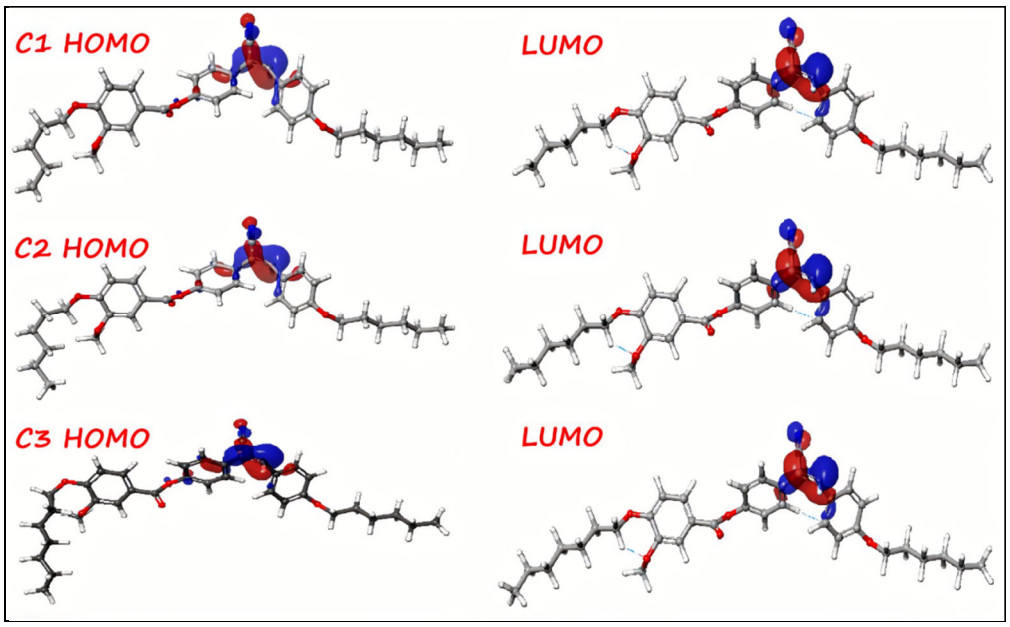

Figure 3. HOMO LUMO of C1 to C3.

The frontier molecular orbital analysis of compounds C1–C3 reveals distinct variations in the electronic distribution with chain elongation. In all three cases, the HOMO is primarily localized over the imine (–CH=N–) linkage and adjacent aromatic donor ring, while the LUMO is concentrated on the electron-deficient aromatic ring bearing the nitrile substituent, confirming the donor–acceptor nature of these systems, as shown in figure 3. In C1, the orbitals are more localized, indicating a relatively larger HOMO–LUMO energy gap. With the increase in alkyl chain length (C2 and C3), the orbitals become more delocalized across the conjugated core, leading to stronger intramolecular charge transfer and stabilization of the π–π conjugation. This progressive delocalization leads to a reduction in the HOMO–LUMO energy gap (C3 < C2 < C1), thereby enhancing molecular polarizability and enabling electronic excitation at lower energies (Figure 3). Such electronic features correlate well with the mesomorphic behavior, as longer chains improve molecular packing and van der Waals interactions, thereby complementing the electronic stabilization observed in the HOMO–LUMO distribution [24-25].

The calculated HOMO and LUMO energies ranged from –0.201 to –0.209 eV and –0.131 to –0.139 eV, respectively, with narrow band gaps (ΔEg) in the range of 0.067–0.070 eV. Among the series, C2 exhibited the lowest energy gap (0.0679 eV), indicating the most favorable charge-transfer interactions and highest electronic polarizability. The chemical hardness (η ≈ 0.034 eV) and softness (S ≈ 0.017 eV^{-1}) values were nearly constant across the series, suggesting comparable stability and reactivity.

Furthermore, the ionization potential (I) increased gradually from 0.201 eV (C1) to 0.209 eV (C3), while the electron affinity (EA) also showed a slight increase from 0.131 eV (C1) to 0.140 eV (C3). This trend implies enhanced donor–acceptor balance and improved electron-accepting ability with longer alkyl chains. Overall, the DFT results confirm that although the alkoxy chain length does not drastically alter the frontier orbital energies, it subtly modulates the band gap, softness, and ICT efficiency [26-30]. These features are favorable for tuning liquid crystalline behavior, optical absorption (red-shifts), and nonlinear optical (NLO) properties in Schiff base derivatives.

Table 1. Density Functional Theory (DFT) analysis of C1 to C3.

Comp-ound	Carbon Chain	E_{HOMO} (eV)	E_{LUMO} (eV)	Δ Egap / E_g (energy gap) (eV)	$\eta = \Delta Eg/2$ (eV)	$S = 1/\Delta Eg = 1/2\eta$ (eV^{-1})	Ionization Potential (I)	Electron affinity (EA)
C1	C5	-0.20146	-0.13167	0.06979	0.03489	0.01744	0.20146	0.13167
C2	C6	-0.20629	-0.13843	0.06786	0.03393	0.01696	0.20629	0.13844
C3	C7	-0.20927	-0.13991	0.06936	0.03469	0.01734	0.20927	0.13991

Note: ΔE_{gap}(Energy Gap) = ($E_{HOMO} - E_{LUMO}$); η = Chemical hardness = ΔEgap/2; S= Chemical softness; *I* = Ionization Potential, EA = Electron Affinity.

4. CONCLUSION

In summary, a new series of liquid crystalline compounds derived from vanillic acid and α,β-unsaturated nitriles were successfully synthesized and characterized through spectroscopic, thermal, and optical studies. The structural confirmation was achieved by ^{1}H NMR, ^{13}C NMR, and FTIR analyses, which validated the formation of the targeted Schiff base derivatives. Thermal investigations by DSC revealed well-defined mesophase transitions, including crystalline to smectic, smectic-to-nematic and nematic to isotropic transformations, with transition temperatures and mesophase stability strongly influenced by the terminal alkoxy chain length. POM observations exhibited characteristic textures such as mosaic, focal-conic, and schlieren patterns, which correlated well with the DSC findings, thereby confirming the mesomorphic behavior. Comparative analysis across the homologous series (C5–C7) demonstrated that elongation of the alkyl chain promoted better molecular packing, enhanced van der Waals interactions, and stabilized the mesophase range. Overall, the study highlights the structure–property relationship in vanillic acid-based Schiff base liquid crystals, providing valuable insights into their design for advanced functional materials.

Conflict of interest

The authors declare no conflict of interest.

Acknowledgments

Authors acknowledged gratitude to the authorities of S.P.T. Arts and Science College and Shri Govind Guru University, Godhra, for providing research facilities and their support.

References

[1] Bhanderi V.D., Katariya K.D., Nakum K. Cyanostilbene-based ester & Schiff base containing liquid crystals: Synthesis, mesomorphic studies and DFT calculations. *Journal of Molecular Liquids* 433 (2025) 127739.

[2] Huijie Yi., Jingjing G., Siyang L., Jiawei M., Jinbao G. Photoresponsive α-cyanostilbene-containing fluorescent liquid crystal polymers based on ring-opening metathesis polymerization for information storage and encryption. *Polymer* 258 (2022) 125289.

[3] Bian L., Zhang J., Wang J., C. Xiaofang Aggregation-Induced Emission-Active Cyanostilbene-Based Liquid Crystals: Self-Assembly, Photophysical Property, and MultiresponsiveBehavior. *Molecules* 29**(**23) (2024) 5811.

[4] Martínez-Abadía M., Varghese S., BegoñaMilián M., Gierschner J., Giménez R., *et al.* Bent-core liquid crystalline cyanostilbenes: fluorescence switching and thermochromism. *Physical Chemistry Chemical Physics* 17 (2015) 11715-11724.

[5] Bala I., Kaur H., Maity M., Yadav R.A., De, J.*, et al.* Electroluminescent Aggregation-Induced Emission-Active Discotic Liquid Crystals Based on AlkoxyCyanostilbene-Functionalized Benzenetricarboxamide with Ambipolar Charge Transport. *ACS Applied Electronic Material***s** 4(3) (2022) 1163–1174.

[6] Martínez-Abadía M., Robles-Hernández B., de la Fuente M.R., Giménez R., Ros M.B. Photoresponsive Cyanostilbene Bent-Core Liquid Crystals as New Materials with Light-Driven Modulated Polarization. *Advance Materials***.** 28(31), (2016) 6586-6591.

[7] Mandle R.J., Gibb C.J., Hobbs J.L. Uncommon building blocks in liquid crystals. *Liquid Crystals* 51(8–9) (2024) 1384–1409.

[8] Nath S., Kappelt A., Spengler M., Roy B., Voskuhl J., *et al.* Tuning the solid-state emission of liquid crystalline nitro-cyanostilbene by halogen bonding. *Beilstein Journal of Organic Chemistry* 17 (2021) 124–131.

[9] Aixiang D., Guiyu Z., Hongbo L.U., Jiaxiang Y. α-Cyanostilbene Derivatives as Fluorescence Liquid-Crystal Molecules: Synthesis and Optical Properties. *Chinese Journal of Applied Chemistry* 31(11) (2014) 1261.

[10] Gong Y., Du C., Wang X., Guo H., Yang F. First stable (Z)-configuration of cyanostilbene derivative: An effective “turn-on“ fluorescent sensor for lysine in aqueous media, *Microchemical Journal* 162 (2021) 105866.

[11] Darji D.P., Pansuriya B.R., Labana B.M., Pandya V.B., Pandya A.D. Influence of substituents on thermal and electronic properties of 4-((E)-phenyldiazenyl)-2-((E)-((4-(alkyloxy)phenyl)imino)methyl)phenol derivatives. *Molecular Crystals and Liquid Crystals* 769 (2025) 418-436.

[12] Panchal J., Mali H., Sharma V.S., Parmar P., Shrivastav P.S., *et al.* Synthesis and characterization of calamitic liquid crystals based on benzothiazole-substituted aroylhydrazone: effect of terminal groups on phase behavior. *Molecular Crystals and Liquid Crystals* 769 (2025) 380-394.

[13] Solanki P., Kholiya K.R., Gohel P.J., Parangi T. Exploring mesophase behavior and biological potential of liquid crystalline Schiff base derivatives of vanilloxy ester: experimental and theoretical studies. *New Journal of Chemistry* 49 (2025) 4085-4098.

[14] Kholiya K.R., Gohel P.J., Solanki P., Kapdiya K., Kamdar J.H. *et al.* Investigation ofphotophysical properties and mesophase behavior in diazenyl-based liquid crystalline aryl cinnamates. *Journal of Molecular Structure* 1341,(2025) 142606.

[15] Waghchoure A.P., Narode H., Sangale V.B., Ali Siddiqui Z., Sarkhel S. *et al.* Assessing the Impact of π-Conjugation Length on Aggregation Induced Emission and Self-Assembly Formation of α-Cyanostilbene and Bis-Cyanostilbene. *Chemistry Select* 9(15) (2024) e202305176.

[16] Igushkina A.V., Golovanov A.A., Vasilyev, A.V. Michael Addition of 3-Oxo-3-phenylpropanenitrile to Linear Conjugated Enynones: Approach to Polyfunctional δ-Diketones as Precursors for Heterocycle Synthesis. *Molecules* 27 (2022) 1256.

[17] Silverstein R.M., Webster F.X., Kiemle D.J. Spectrometric Identification of Organic Compounds, 7th Edition, Wiley (2005).

[18] Brian C. Smith. Organic Nitrogen Compounds IV: Nitriles. Spectroscopy 34(7) (2019) 18–21.

[19] Lin C., Qin J., Zhang Y., Ding G. Diagnostically analyzing 1H NMR spectra of sub-types in chaetoglobosins for dereplication. *RSC Advance* 10 (2020) 1946-1955.

[20] Kumar S. *Liquid Crystals: Experimental Study of Physical Properties and Phase Transitions.* Cambridge University Press (2001).

[21] Tschierske C. Development of structural complexity by liquid-crystal self-assembly. *Angewandte Chemie International Edition* 52(34) (2013) 8828–8878.

[22] Destri S., Pasini P., Semeria M. Thermotropic liquid crystalline behavior of Schiff bases derived from substituted hydroxybenzaldehydes and aniline derivatives. *Liquid Crystals* 25(5) (1998) 611–617.

[23] Rao D.S.S., Sadashiva B.K. The effect of alkyl chain length on the mesomorphic behaviour of some Schiff base esters. *Journal of Materials Chemistry* 2 (1992) 767–771.

[24] Frisch M.J., Trucks G.W., Schlegel H.B., Scuseria G.E., Robb M.A., *et al.* Gaussian 16, Revision C.01, Gaussian, Inc., Wallingford CT (2016).

[25] Dennington R., Keith T.A., Millam J.M. GaussView, Version 6.1, Semichem Inc., Shawnee Mission, KS, 2016.0 (2016).

[26] Petrou P.S., Nicolaides A.V. Electron affinities of a homologous series of tertiary alkyl radicals and their C–H bond dissociation energies (BDEs). *Tetrahedron* **65**(8) (2009) 1655-1659.

[27] Silva A.L.R., León G.P., Lukeš V., Klein E., Ribeiro-da-Silva M.D.M.C. Thermodynamic Properties of γ- and δ-Lactones: Exploring Alkyl Chain Length Effect and Ring-Opening Reactions for Green Chemistry Applications. *Molecules* 30 (2025) 399.

[28] Xu F., Matsumoto K., Hagiwara R. Effects of alkyl chain length on properties of 1-alkyl-3-methylimidazolium fluorohydrogenate ionic liquid crystals. *Chemistry* **16**(43) (2010) 12970-12976.

[29] Alamro F.S., Ahmed H.A., Bedowr N.S., Khushaim M.S., El-Atawy M.A. New Advanced Liquid Crystalline Materials Bearing Bis-Azomethine as Central Spacer. *Polymers* 14(6) (2022) 1256.

[30] Li J., Wang Z., Deng M., Zhu Y., Zhang X., *et al.* General phase-structure relationship in polar rod-shaped liquid crystals: Importance of shape anisotropy and dipolar strength. *Giant* 11 (2022) 100109.